

DMTG: A Human-Like Mouse Trajectory Generation Bot Based on Entropy-Controlled Diffusion Networks

Jiahua Liu

University of Michigan, USA
Email: jiahual@umich.edu

Zeyuan Cui

Email: zeyuancui@hotmail.com

Wenhan Ge

College of Computer Science
Sichuan University, China
Email: saltriangle@163.com

Pengxiang Zhan

College of Computer Science
Sichuan University, China
Email: hanpengxiang@stu.scu.edu.cn

Abstract—CAPTCHA protects normal business and prevents resource misuse and data theft by distinguishing between human operations and machine programs in the network. Advances in machine learning techniques have made traditional image-based and text-based CAPTCHAs susceptible to targeted attacks, thus modern CAPTCHAs such as GeeTest and Akamai incorporate behaviors such as mouse track detection for senseless detection. Present methods for bypassing mouse behavior detection mainly implement simulation generation of mouse trajectories through representation learning, adversarial learning, or reinforcement learning. Such methods suffer from the difficulty of fully mimicking human style and the lack of all-round testing, which makes it challenging to evaluate the effectiveness of anti-bot measures. To address these issues, this paper proposes a mouse trajectory generation and evaluation framework based on an entropy-controlled diffusion model: DMTG, which accepts complexity control and generates mouse control curves approximating real human samples. The framework also provides both white-box and black-box testing methods for verifying whether the model can have the ability to obfuscate human-machine operations and pass the online commercial CAPTCHA test. The experiments are centered around black-box and white-box tests. In the white-box tests, DMTG has a significantly lower probability of being detected as a bot than the other models, as evidenced by an average 4.75% to 9.73% reduction in the bot recognition accuracy, and 5.11% to 10.51% in macro F1s. Additionally, we evaluated the performance of the DMTG framework on commercial CAPTCHA systems to assess its effectiveness in real-world scenarios. Due to copyright and proprietary restrictions, detailed results are not provided in this paper. Furthermore, DMTG can effectively mimic the physical properties of human operations, including slow initiation and differences in applied force for different directions. The results show that DMTG is more likely to generate mouse trajectories in human expectations and can provide quantitative simulation metrics.

1. Introduction

CAPTCHA (Completely Automated Public Turing test to tell Computers and Humans Apart) [1] distinguishes human and automated mechanical operations through complex logic to prevent large-scale data theft and misuse. Traditional CAPTCHA methods are based on image [2], [3], text [4], [5], [6], and other medias. Due to the development of Artificial Intelligence (AI), these CAPTCHAs can be easily bypassed through large-scale supervised learning. For example, CNN [2] or YOLO [7] recognition can locate image elements. Large Language Models (LLM) [8] are good at reading comprehension or solving logical judgments. As a result, many advanced CAPTCHA advocate developing invisible detection, such as the mouse or finger trajectory or other behaviors.

1) **Style Variation**: Existing methods face challenges in achieving controllable random generation of mouse trajectories that cater to the distinct styles of different operators. 2) **Real-World Applicability**: Current approaches primarily rely on white-box testing and quality evaluation metrics like accuracy, lacking sufficient experimentation in large-scale real-world CAPTCHA black-box environments. This limitation weakens the robustness and generalizability of most methods.

Since dual unknowns of the data and the model, the mouse trajectory behavior detection methods for most commercial CAPTCHAs are in a black box.

Existing methods for obfuscated generation of mouse trajectories mainly include adversarial or reinforcement learning [9], [10], [11], [12], and encoder-decoder [13], [14]. Most of these methods rely on simulated adversarial environments in laboratory settings and lack evaluations in real-world network scenarios. Their issues primarily include the following two points. 1) **Anthropomorphic Stylization**: Existing methods struggle to generate mouse trajectories that are tailored to different web pages and user styles, making them easy to track and trace; 2) **Practical Testing**

Limitation: Current approaches primarily rely on white-box testing and evaluation metrics like accuracy, lacking sufficient black-box experimentation of large-scale real-world CAPTCHA environments. This limitation weakens the robustness and generalizability of most methods.

We propose DMTG (Diffusion-based Mouse Trajectory Generator), an end-to-end approach for generating realistic mouse trajectories based on the theory of entropy-controlled DDIM [15]. Entropy-controlled DDIM adjusts the local uncertainty of generated mouse trajectories by an energy coefficient, allowing the trajectories to exhibit human-like randomness while achieving controlled objectives. Compared to prior works, the primary innovation of DMTG lies in its “**controllable randomness**”. On the one hand, due to the diffusion process, identical web pages yield differing trajectories in each generation turn, which adapts to humans’ unpredictability. On the other hand, the constraints imposed by the style transfer module enable DMTG to mimic and clone the user’s historical behaviors relatively, thereby blurring the distinctions between human and machine operations.

The main contributions of this paper are as follows:

- We introduce the DMTG framework, which can generate highly realistic mouse trajectories to bypass the CAPTCHA detectors.
- We improve the DDIM model using information entropy theory, enabling users to control trajectory length, complexity, and target position.
- We propose white-box testing methods including distribution measurement and deep learning prediction to assess the fundamental differences between simulated mouse trajectories and human activities.

The rest of the paper is structured as follows: **Sect. 2** presents the current approaches of CAPTCHA and Generative Artificial Intelligence (GAI). **Sect. 3** describes the modeling and methodology of DMTG. **Sect. 4** discusses the experiments and interpretations. **Sect. 5** summarizes the whole paper and mentions our future works.

2. Related Work

This section will present the current state of research on existing CAPTCHA technology schemes and GAI, which provide the knowledge base and comparison methodology for DMTG.

2.1. CAPTCHA and Deceivers

Existing CAPTCHA [1] can be divided into four basic categories: text-based, image-based, audio-based and user behavior-based. Text-based CAPTCHA verifies whether the user has entered the correct text string using distorted or noisy text images to distinguish between automated programs and real humans [4], [5], [6]. Image-based CAPTCHA synthesizes the logical differences between humans and machines through image semantic understanding [2], [3]. For example, Tencent’s VTT [16] uses style migration in conjunction with 3D shapes to generate check

images. Google’s reCAPTCHA [17] uses adversarial perturbations to interfere with AI’s recognition of images to distinguish humans from bots. CAPTCHA based on phonetic or biological information uses voiceprint or timbre to differentiate between human and synthetic speech [18], which is less common than images and text.

CAPTCHAs based on images, text, and sounds are significant because these verification methods can provide an obvious target for the screening object to process. The AI robot can be purposefully simulated to bypass these filters because of their strong willingness [19]. For example, Deng et al. [8] exploited the cross-domain logic capabilities of LLMs to bypass image understanding tasks. Hossen [20] uses YOLOv3 [21] to locate elements in reCAPTCHA v2. Wang [22] prefers the word obfuscation-generating units combined with Recurrent Neuronal Networks (RNN) [23], Convolutional Neural Networks (CNN) [24], and attention mechanisms [25] to achieve Chinese validator bypass. Due to the vulnerability of explicit CAPTCHA to attacks, CAPTCHA based on implicit user behavior verification has been chosen as a new type of verifier.

The implicit nature of the user behavior CAPTCHA is reflected in the black-box nature, including the unnoticeable, unknowable, and unrepeatable attributions in detection. Mouse2Vec [26] uses the Transformer self-supervised framework for learning semantic representations of mouse behavior. ReMouse [27] provides novel real-world mouse dynamics datasets and finds that the irreducible nature of human manipulation can be used to circumvent replayed machine simulation behavior. Acien [28] uses RNN for gesture recognition to realize user touch behavior detection of smartphones. Jin [29] uses CNN and RNN to distinguish human and machine mouse trajectories. T-Detector [14] uses RNN and CNN to model human-computer operational differences in gaming scenarios and finds that humans have more ineffective activities. As a long-term detection process, the mouse track CAPTCHA is considered to have a certain degree of review and correction capabilities. This makes the attack robots facing it relatively more complicated and requires considering the accumulation of multiple factors.

The invisibility and complexity of user behavior CAPTCHAs make mouse trajectory attacks in their infancy. Existing methods focus on using distribution fitting to generate behaviors of fake humans to bypass the detection. BeCAPTCHA-Mouse [9] uses Generative Adversarial Networks (GAN) [30] to generate mouse trajectory distributions that mimic those of humans. Folch [31] uses a hybrid mechanism of multiple straight lines and curves to simulate and detect the robot mouse operation trajectory. SapiAgent [13] uses an auto-encoder to simulate human operations. CC-Net [12] designed a set of image- and text-based multimodal network-generated basic sequences of computer operations and outperformed on the MiniWob++ [32] test. Tsingenopoulos [11] designed an automated web browser based on Reinforcement Learning (RL) [33] to bypass the behavioral scoring mechanism of reCAPTCHA v3, and found that if humans are involved in initiating the browsing, the subsequent non-human operating agent

is extremely difficult to detect.

Summarily, among all CAPTCHAs, user behavior detection can provide the website with the greatest protection against machine abuse. Although the existing solutions to bypass user behavior detection mostly use adversarial generation to promote robots to imitate humans, there are still some problems in track generation: 1) **Anthropomorphic Stylization**. The non-repeatability of human operations found by ReMouse [27], the ineffective human operation characteristics found by T-Detector [14], and the human hot-start bypassing found by Tsingenopoulos [11], all show that there is still room for improvement in existing mouse track generation schemes. Thus, the new type of mouse trajectory generation needs to imitate the randomness of human operations and the historical styles of different humans to form an attack scheme with inconspicuous differences. 2) **Practical Testing Limitation**. Although some solutions have passed the reCAPTCHA experiment, they still need to be more widely verified in a variety of commercial CAPTCHAs.

2.2. Generative Artificial Intelligence

GAI creates creative, hard-to-code, clear, persuasive, and relatively versatile text or visual output based on large amounts of training data, augmenting the capabilities of existing human workers by increasing productivity and bringing greater efficiency to repetitive editing tasks [34]. Modern GAI tasks mainly focus on fields like sequences (video, text, audio), images/graphics, and chemistry/biomedicine, aiming to generate working modes or result distributions that are close enough to humans [35]. These tasks mainly rely on four frameworks: Encoder-Decoder [36], [37], [38], [39], GAN [30], [40], [41], [42], Transformer [25], [43], [44], [45], and Diffusion Network [46], [47], [48]. These four architectures can be grouped according to the global distribution and local context of modeling. Among them, Encoder-Decoder and GAN are typical global sampling, which advocate representing the input as an independent distribution and resampling it as new data. While Transformer and Diffusion Networks follow local context sampling, which cumulatively obtains new data whose elements are related to each other through time-step changes.

As discussed in **Sect. 2.1**, existing mouse trajectory generation methods mainly employ GANs and Encoder-Decoder architectures. These architectures are prone to biases in local features, resulting in identification as robotic behavior. And we believe that Transformer and Diffusion Networks can correct such local disparities. Therefore, we will focus on discussing the current state of Transformer and Diffusion Networks here.

Although both Transformer and Diffusion Networks reason through context, there is a dimensional difference. Transformer performs contextual vacancy reduction more through spatially consistent logic. For example, ViT [43] and DALL-E [45] can generate scene-dependent images from the positional encoding and pixel content of image patches. GPT [44] and LLaMA [49] are good at generating subsequent words with the help of conditional transfer probabilities

from the preceding content of the text. While Transformers demonstrate efficient information-gathering capabilities, they still pose risks of forgetting in ultra-long, infinite, or cross-domain scenarios [50]. At the same time, because Transformer’s original models are generally large and complex, it is difficult to balance its computational efficiency and accuracy [51]. These requirements constrain the deployment of Transformer to low-resource computing devices, making the computational cost difficult to control.

Diffusion Network generates special results from noise by utilizing thermodynamic diffusion principles and their inverse processes on time slices [46]. Compared to the Transformers, Diffusion Networks better represent the continuity of frames and states. For example, DDPM [47] implements a deep diffusion model fitting method for generating high-quality images of the same subject. AlphaFold3 [48] utilizes a diffusion model to generate the folded spatial structure of a protein macromolecule. MedSegDiff [52] has designed a DDPM-based U-Net [53] architecture for segmenting regions in medical images. UniDiffuser [54] presents a multi-distributed diffusion model for generating realistic text or images that rival customized large-scale Transformer capabilities while maintaining efficiency, demonstrating the potential of Diffusion Networks. Current challenges in Diffusion Networks focus on the distribution, direction, process, and feedback controllability of generation [55], [56], [57] so that researchers still have room for improvement in locally customized generation.

3. Methodology

3.1. Issue Definitions

As discussed in **Sects. 1** and **2.1**, DMTG primarily revolves around two objectives: **Anthropomorphic Stylization** and **Practical Testing Limitations**, in realistic mouse trajectories generation. Anthropomorphic stylization necessitates GAI to mimic human habits, demeanor, and even errors in trajectory generation. Practical testing limitation requires the generated mouse trajectories to circumvent generic commercial-grade CAPTCHA detectors. To address these, we need to tackle three fundamental Research Questions (RQ):

RQ1 How to construct mouse trajectories that are simultaneously compatible with randomness and purposiveness?

RQ2 How to ascertain that such trajectories adhere to human operational styles, making them indistinguishable from those of the other bots?

RQ3 How to evaluate the model’s ability to bypass commercial CAPTCHAs?

Our method consists of the following main 4 steps:

Step-1. Data collection: we use the SapiMouse dataset [58] and the Open Images V7 dataset [59] as our training datasets, which contain samples of human mouse shenanigans.

Step-2. Model Construction: the goal of DMTG is to mimic human trajectories, and thus RQ1 and RQ2 need to be solved. The RQ1 is solved by the main body of the DMTG’s entropy-controlled diffusion networks named α -DDIM. And RQ2 is controlled by the DMTG’s unique loss function. Both RQ1 and RQ2 requires that the α -DDIM be able to generate directional trajectories from random seeds, implying that the trajectory \hat{Y} -generation function:

$$\hat{Y} = f(\vec{X}, \epsilon, \alpha, m) \quad (1)$$

needs to have 4 inputs, the target directions \vec{X} of the start and end of the mouse movement, the random initial noise ϵ , the complexity control factor α to terminate the diffusion progress, and the node num m that control the action frames of the whole trajectory.

Step-3. System Development: α -DDIM only realizes the core functionality of the DMTG system, in order to realize a usable system, it is necessary to add: fingerprint assembler, peripheral controllers, and other supporting facilities.

Step-4. Evaluation: we designed black and white box tests separately. The white box identifies authentic trajectories by constructing a fully supervised AI model to evaluate RQ2. While the black box testing utilizes commercial CAPTCHA to test bypass rates to answer RQ3.

The remaining sub-sections of this section will illustrate how DMTG is implemented and address the posed RQs.

3.2. Data Collection

The dataset used by DMTG is a mixture of the SapiMouse dataset [58] and the Open Images V7 dataset [59]. SapiMouse collected human mouse trajectories from 120 participants, where the data is in the form of a set of coordinates along with corresponding timestamps containing mouse events. Open Images V7 provides annotations for semantic understanding of images. We utilize the sequences of mouse coordinates under the “traces” label in Open Images. After combining these coordinate data, we randomly sampled 1 million instances as human samples to train the robot’s modeling capability.

3.3. Model Construction

The DMTG framework has two components: a generator for generating controlled random trajectories, and a series of raters for evaluating bypassing and imitation capabilities. The structure of the whole framework is shown in Fig. 1. The generator consists of two main functions, the initialization to formulate the mouse agent task, and the α -DDIM to generate “controlled random” trajectories in RQ1. Besides, we design a Browser Proxy Bot for simulating real operating environments and deployed the α -DDIM model. The quality evaluators also have two components. The Simulation Confidence Assessments answer the human

imitation ability assessment in RQ2, and The Commercial CAPTCHA Validations measure the generalizability and real-world applicability in RQ3.

Suppose an arbitrary mouse coordinate is $p = \langle x, y \rangle$ s.t. $x \in [0, W], y \in [0, H]$, where W is the width of the screen and H is the height of the screen. Then a mouse track with m moves can be represented as a set of mouse coordinates with $m + 1$ nodes: $\{p\}_{m+1} = \{\langle x_0, y_0 \rangle, \langle x_1, y_1 \rangle, \dots, \langle x_m, y_m \rangle\}$. In this set, $p_0 = \langle x_0, y_0 \rangle$ is the initial position of the mouse and $p_m = \langle x_m, y_m \rangle$ is the final position. Thus the \vec{X} can be expressed as $\vec{X} = \{p_0, p_m\}$.

For a mouse control that is specified to move m times, a simple approach is to move directly from $\langle x_0, y_0 \rangle$ through the same m displacements in the direction of \vec{X} , with each displacement $\frac{\langle x_0, y_0 \rangle - \langle x_m, y_m \rangle}{m}$. A complex method is to apply completely random coordinates for the first $m - 1$ turns of the m displacements and then move directly to $\langle x_m, y_m \rangle$ for the last one. However, whether it is the simple or the complex one, it reveals that an automated program controls the mouse because the track does not conform to human operating habits. So we need to make the mouse trajectories between the two, to achieve a relative balance between purposefulness and randomness.

Based on this goal, it was easy to think of using DDIM [15] for generating mouse trajectories. DDIM is based on the inverse process of the thermodynamic entropy increase phenomenon and can generate all the transition states and ways of changing from completely random to direct utilizing neural networks. Thus, DDIM can generate human-like states at some point, allowing DMTG to generate highly realistic mouse trajectories. However, existing DDIMs fail to meet our requirements for controlling curve complexity. Therefore, we need to modify the model accordingly to archive α -DDIM.

3.3.1. Mouse Trajectory Initialization. In the initialization phase we need to complete the initialization of the three base parameters in Sect. 3.3.1. Since each generation process of the α -DDIM is a stepwise denoising process, the initial input to the model should be a randomized mouse trajectory. We use normal random as our noise initialization function: $\epsilon \sim \mathcal{N}(0, \Sigma_\epsilon)$, where Σ_ϵ is its standard deviation which is given by Eq. (2).

The point $p_c = \langle x_c, y_c \rangle = \langle \frac{x_0 + x_m}{2}, \frac{y_0 + y_m}{2} \rangle$ here denotes the midpoint between the starting point $\langle x_0, y_0 \rangle$ and ending position $\langle x_m, y_m \rangle$. Here k_c is the scaling factor. According to the density function of the normal distribution, 3 times the covariance can make the probability of being within the screen 99%. Therefore, the scaling coefficient k_c is generally taken to be $\frac{1}{6}$.

$$\Sigma_\epsilon = ((k_c(x_m - x_0))^2 + (k_c(y_m - y_0))^2) \begin{bmatrix} 1 & 0 \\ 0 & 1 \end{bmatrix} \quad (2)$$

Since DDIM network cannot handle continuous inputs, necessitating downsampling into discrete points. Also due

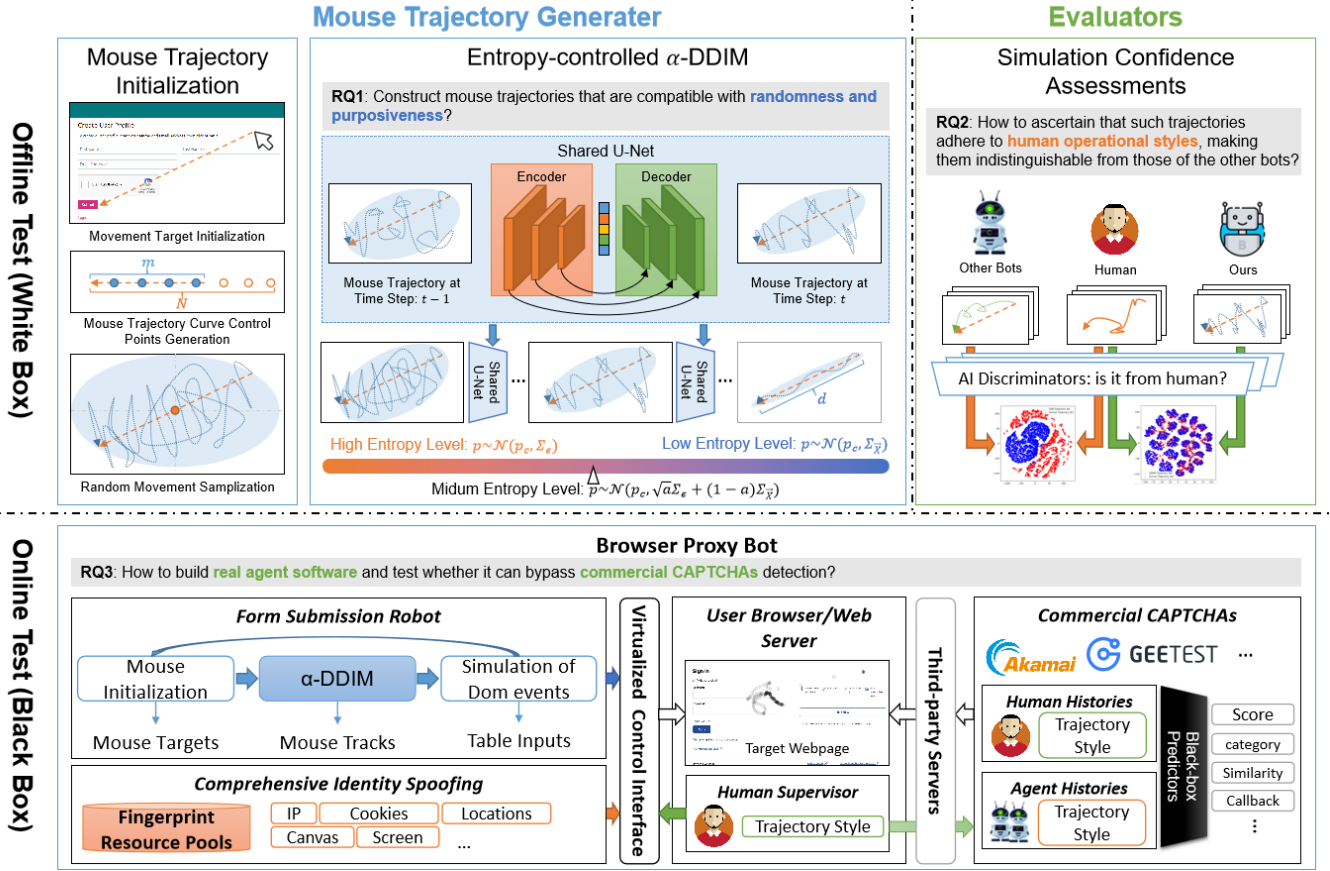


Figure 1. DMTG Framework

to the limitation of the number of sampling points m in , the final input X_R is defined by **Eq. (3)**.

$$X_R = \{\langle x_0, y_0 \rangle\} \parallel \{p_c + \epsilon_i\}_{i=1}^m \parallel \{\langle x_m, y_m \rangle\} \parallel \{\langle 0, 0 \rangle\}_{N-m} \quad (3)$$

where $0 < m \leq N$ represents the generated length, and \parallel denotes the concatenation symbol. N is the max length limited by models. Simultaneously, to ensure that the input length remains unchanged, we will append $N - m$ masks $\langle 0, 0 \rangle$ in the subsequent steps.

3.3.2. α -DDIM Framework. First, we need to understand that there are 2 extreme phases within the original DDIM generation cycle. One is complete randomness and the other is complete order. Complete randomness occurs at the initialization stage of the mouse trajectory, when the points in the curve X_R are all independently Gaussian-distributed sampling points, such as **Eq. (2)**. Complete order occurs at the decoding endpoint of the DDIM, when all points in the curve X_R tend to line up in the vector direction of \vec{X} , forming a set of straight line segments, e.g., **Eq. (5)**. Neither of these extremes is desirable; what we want is a “controlled randomness”, somewhere in the middle of the DDIM generation cycle, that is neither too orderly nor too

chaotic. Therefore, we can use a mixture of both Gaussian distributions to represent the sampling, e.g., **Eq. (4)**.

$$p_\alpha = p_c + \epsilon_\alpha \quad (4)$$

$$s.t. \epsilon_\alpha \sim \mathcal{N}(0, a\Sigma_\epsilon + (1-a)\Sigma_{\vec{X}}), 1 \geq a \geq 0$$

$$\Sigma_{\vec{X}} = \begin{bmatrix} (k_c(x_m - x_0))^2 & k_c^2(x_m - x_0)(y_m - y_0) \\ k_c^2(x_m - x_0)(y_m - y_0) & (k_c(x_m - x_0))^2 \end{bmatrix} \quad (5)$$

$$q_\sigma(p_a | \vec{X}) := \mathcal{N}(p_c; a\Sigma_\epsilon, (1-a)\Sigma_{\vec{X}}) \quad (6)$$

$$\simeq \mathcal{N}(p_c; \sqrt{a}\Sigma_\epsilon, (1-a)\Sigma_{\vec{X}})$$

$$= \mathcal{N}(p_a; \sqrt{a}\Sigma(\vec{X}), (1-a)\Sigma(X_R))$$

It is worth noting that the human-like trajectory we need in **Eq. (5)**, can be approximated by the original process of DDIM [15], with the inference process shown in **Eq. (6)**. Where, the required a serves the same purpose as DDIM’s α_t . $\Sigma(\cdot)$ is the function that calculates variance. The status of \vec{X} is the same as the original requirement of x_0 in DDIM, both symbolizing the structured data; while the role of X_R is analogous to that of DDIM’s I , representing complete noises.

Based on the assumption that the information entropy $H(\{p_a\})$ of the set of points p_a of any controlled curve can be calculated as **Eq. (7)**.

$$\begin{aligned} H(\{p_a\}) &= \frac{1}{2} \log((2\pi e)^2 |a\Sigma_\epsilon + (1-a)\Sigma_{\bar{X}}|) \\ &= \log(2\pi e) + \frac{1}{2} \log(|a\Sigma_\epsilon + (1-a)\Sigma_{\bar{X}}|) \end{aligned} \quad (7)$$

Although, we tend to control the entropy of the curve output from the model to control the complexity of the trajectory, this may not be easy. This is because, although there is a constraint on the mixing parameter a of the mixed Gaussian distribution, the value of this a cannot be confirmed, resulting in $H(\{p_a\})$ not being available. We therefore thought of replacing the computation of $H(p_a)$ by utilizing an approximate solution that can be used to reflect the complexity of the curve in the iteration.

We do this by utilizing the total length of the curve as a replacement. In fact, there is theoretical support for this approach. For the total length of a curve, it is always greater than or equal to the length of the Minimum Spanning Tree (MST) of the point set p_a . At the same time, controlled randomness also requires that the mouse trajectory be relatively smooth, so that the total length of the curve is ideally equal to the length of the MST as in **Eq. (8)**.

$$L(\{p_a\}) = \sum_{i=1}^m \|p_a^{(i)} - p_a^{(i+1)}\|_2 \simeq L_{MST}(\{p_a\}) \quad (8)$$

The logarithm of the mathematical expectation of MST length is positively related to $H(\{p_a\})$. The mathematical derivations are shown in **Eq. (9)** where β is a constant associated with $|a\Sigma_\epsilon + (1-a)\Sigma_{\bar{X}}|$. Our simulation results in **Fig. 2** prove this point.

$$\begin{aligned} &\log(\mathbb{E}(L_{MST}(\{p_a\}))) \\ &\simeq \log(\beta \sqrt{m |a\Sigma_\epsilon + (1-a)\Sigma_{\bar{X}}|}) \\ &= \log(\beta) + \frac{1}{2} \log(m) + \frac{1}{2} \log(|a\Sigma_\epsilon + (1-a)\Sigma_{\bar{X}}|) \\ &= H(\{p_a\}) + \log(\beta) + \frac{1}{2} \log(m) - \log(2\pi e) \end{aligned} \quad (9)$$

Based on the above arguments, we can basically conclude that the controlled randomness we want is related to the total length of the mouse trajectory. Therefore we will input the length of the curve we wish to form normalized as α coefficients into α -DDIM to participate in the complexity control of the curve. The diffusion process of the DDIM stops and the output of the generated trajectory is output when, and only when, the curve length normalized at a certain point in time is equal to the preset α . These processes can be obtained by adding α constraints to the original formulation of the DDIM.

We employ the U-Net framework to implement $f_\theta(X_{t-1}|X_t, \alpha)$. The architecture of this model is depicted in **Fig. 3**, comprising $2 \times A$ layers of encoding and decoding

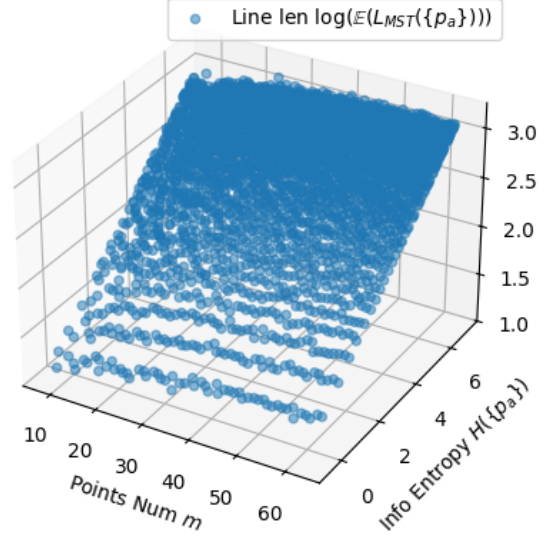


Figure 2. Simulation Results of Points Num m , Info Entropy $H(\{p_a\})$, and MST Length $\log(\mathbb{E}(L_{MST}(\{p_a\})))$

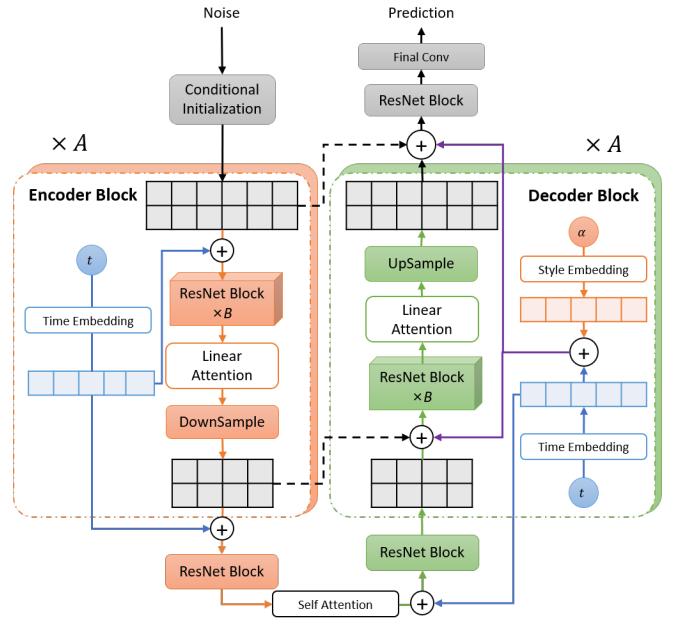


Figure 3. U-Net Model for α -DDIM

units. In this architecture, the decoding units are influenced by the time step t and the complexity control coefficient α to encode high-dimensional vectors. In contrast, the encoder layers are solely controlled by the time step t to control the iteration rounds. Furthermore, residual connections exist between encoding and decoding layers of the same dimensions to prevent gradient vanishing.

The time embedding in the model utilizes positional encoding similar to the Transformer model [25]. The style encoding (**Eq. (10)**) corresponds to the complexity control

coefficient α . Where, $1/(\alpha+1)$ is responsible for transforming the range of α from $[0, +\infty)$ to $(0, 1]$. $\lfloor \cdot \rfloor$ denotes the floor function, which assigns the style to one of S categories. $PosEmb(\cdot)$ represents the positional encoding.

$$\begin{aligned} StyleEmb(\alpha) &= PosEmb(\lfloor \alpha S \rfloor) \\ s.t. \quad \alpha &= 1/(\alpha + 1) \end{aligned} \quad (10)$$

3.3.3. α -DDIM Losses. The loss function for the trajectory generation process consists of 3 components. The first component is the original loss function of DDIM, denoted as L_{DDIM} in **Eq. (11)**. Secondly, $L_{sim}(\theta)$ constrains the gap between the human trajectory \hat{X} and the machine trajectory p_a , as shown in equation (12). The third component is the style loss L_{style} , responsible for providing constraints on α_t , as illustrated in **Eq. (13)**. Where, α represents the theoretical complexity input into the model. The final loss L is the sum of these components. w_1, w_2 and w_3 are the weights.

$$L_{DDIM} := \mathbb{E}_{\vec{X}, \Sigma_\epsilon} \left[\|\Sigma_\epsilon - \Sigma(\sqrt{a}\vec{X} + \sqrt{1-a}\Sigma_\epsilon)\|_2 \right] \quad (11)$$

$$L_{sim} := \|p_a - \hat{X}\|_2^2 \quad (12)$$

$$L_{style} := \left\| \alpha - \frac{\sum_{i=1}^m \|p_a^{(i)} - p_a^{(i+1)}\|_2}{\|p_0 - p_m\|_2} \right\|_2 \quad (13)$$

$$L = w_1 L_{sim}(\theta) + w_2 L_{sim} + w_3 \cdot L_{style} \quad (14)$$

3.4. Evaluation

3.4.1. Simulation Confidence Assessments. This subsection discusses solving RQ2 (White-box testing), which proposes to evaluate how well our model can generate the most human-like mouse trajectories. We devised two tests, one utilizing a distribution distance metric function and the other using a deep learning-based discriminator. The distribution distance metric measures the degree of similarity between the model-generated results and real human samples. The deep learning-based discriminator can find and amplify the small differences between the two trajectories and is more capable of determining whether the model simulates human operating habits in all aspects.

For ease of comparison, we will employ three sets of samples for measurement:

- 1) **Human samples:** randomly sampled from collected human operation data.
- 2) **DMTG samples:** multiple generation processes initialized based on each human sample, with one simulation result randomly selected from the outcomes.
- 3) **Samples from other models:** an equal number of samples generated will be chosen from comparative generation models in the experiments.

For distribution analysis, a variety of similarity and distance measurement methods will be employed, including Jensen–Shannon Divergence (JSD) [60], Earth Mover’s

Distance (EMD) [61], [62], MSE, Root Mean Square Error (RMSE), Cosine Similarity (CosSim), and so on. These metrics will assess the disparities between model-generated mouse trajectories and human trajectories from multiple perspectives, such as curve density, mean, and distribution. Because our DMTG can control trajectory curves by complexity and length parameters, we will extract and scale the effective region during testing. Additionally, due to the bivariate Gaussian distribution nature of mouse trajectory data, which may complicate the computation of metrics like JSD, we will employ t-SNE [63] to map high-dimensional curves to single-point vectors for computing.

For deep learning metrics, we designed two scenarios for robot recognition: unified and independent. The objective of the independent scenario design is to measure the degree of overlap between human and machine trajectories in data distribution. In this scenario, we employ randomly selected 7 sets of human and separate model samples as positive and negative samples, respectively, for training the discriminator to verify its recognition capability on the remaining 3 sets of samples. For the unified recognition scenario, we aim to demonstrate the effectiveness of our model in a global environment. Therefore, we construct a dataset with equal distribution comprising all human samples, DMTG samples, and samples from other models. The dataset is split into training and testing sets at a ratio of 7:3, to validate whether the discriminator can detect robot samples in the testing set.

3.4.2. Commercial CAPTCHA Validations. The primary bypassed commercial CAPTCHAs in this test are Akamai [64], GeeTest [65], and reCAPTCHA v3 [17]. Akamai assigns a unique token to each session, collecting and uploading interaction data related to each web page operation to update the underlying confidence level of the session and determine whether to allow the request. Since the internal confidence level of Akamai cannot be known, only a signal indicating whether the test was passed will be returned. Therefore, experiments with Akamai will evaluate both the time taken to pass the test and the number of times the test is passed. The evaluation score is calculated using **Eq. (15)**, where T is the theoretical time required for executing the trajectory, and t_a is the execution time of the testing program. If no pass signal is issued after the trajectory execution is completed, the test is considered not to be passed. The final passing score will be the average score from multiple tests.

$$S_{Akamai} = ReLU\left(\frac{T - t_a}{T}\right) \quad (15)$$

Geetest predicts and returns a confidence score of 1 to 6 for each attempt by the user to solve the CAPTCHA challenge, with higher scores being considered closer to human operation. Since we can access such scores, the average score over multiple attempts will be used as the evaluation.

reCAPTCHA v3 uses IP credits and Google-related cookies for human-computer testing, and the product will return scores in the range of 0.1 to 0.7. In our testing, we

found that mouse trajectory is not a significant factor for reCAPTCHA v3, and even human users received similar scores.

4. Experiments

This section will focus on experimental validation for RQ2 and RQ3, and will construct the experimental methodology following the process described in Sects. 3.4.1 and 3.4.2. The comparative model for word experiments is as follows.

- **GAN:** BeCAPTCHA-Mouse [9] utilizes GAN networks to simulate human mouse trajectories for detecting robot operations.
- **SapiAgent:** SapiAgent [13] employs the SapiMouse [58] dataset and a deep encoder architecture for CAPTCHA deceptive bypass.
- **Bezier:** Bezier [66] is a method based on generating smooth curves using multiple anchor points.
- **Linear:** This method, discussed in Sect. 3.3, simply employs a control approach using N equidistant points along the \vec{X} direction.
- **Ghost:** Ghost-cursor [67] dynamically adjusts the displacement velocity between mouse trajectory curves and operating DOM elements using Fitts' Law to create realistic behavior. This method represents a relatively successful engineering case.

The deep learning trajectory discriminators in Sect. 3.4.1 will be implemented using Decision Tree (DT) [68], Random Forest (RF) [69], XGBoost (XGB) [70], Gradient Boosting (GB) [71], MLP [72], CNN [24], RNN [23], LSTM [73], BiLSTM [74], and TCN [75]. Each discriminator will carry out experiments on all comparison models and DMTGs separately following the methods involved in Sect. 3.4.1. All the deep learning models are built using PyTorch and trained on a Nvidia A100 GPU.

Before formal testing, we wish to determine which complexity configuration can more easily yield human-like curves. Therefore, we analyzed the influence of different values of α in Eq. (10) based on human datasets. The results are shown in Fig. 4 and Table. 1. According to the results, we found that when $\alpha \leq 0.2$, the generated curves exhibit excessively high randomness. While when $\alpha \geq 0.8$, the generated curves tend to approximate a straight line. The optimal curves correspond to α values between 0.2 and 0.3. Hence, we will use random values ranging from 0.3 to 0.8 as α for the subsequent experiments.

4.1. RQ2: Simulation Confidence Assessments

Tables. 2 and 3 respectively present the prediction accuracy and other metrics of human and machine trajectories using unified and independent discriminators. For each test, every model generates a sample size of 1 million for random selection. Higher accuracy indicates that the model curves and true mouse trajectories are more easily distinguishable by the discriminator. Therefore, lower scores in the table indicate that the generated curves by the models have smaller

differences in features compared to human operations. The following conclusions can be drawn:

- 1) **DMTG performs the best among models.** Various discriminators show the lowest prediction accuracy for our DMTG model, approximately 10% lower than other confusion methods. This indicates that our trajectories are most prone to confusion with human actions, thereby misleading the discriminator to make incorrect classification predictions. Although Ghost can also provide trajectories that are easily misclassified, its confusion strength is much weaker than DMTG.
- 2) **DMTG does not introduce additional errors.** Although visually and intuitively, GAN and SapiAgent can generate highly complex and sufficiently simulated curves, their trajectories are significantly more likely to be discovered than Bezier and Linear. This indirectly reflects that these curves cannot reliably reflect the distribution of real mouse trajectories. Instead, they are more easily discovered due to the introduction of more obvious trajectory noise.
- 3) **DMTG is more suitable for online detection scenarios.** When using independent detectors, the discriminator's recognition accuracy for DMTG is around 90%; however, when using a unified detector, the accuracy drops to around 80%. Under the same conditions, Ghost's accuracy drops from around 92% to 90%, and the average accuracy of other models drops from 99% to 95%, with reductions of less than 10% on average. This indicates that if online detectors use multiple judgment methods for black-box testing, similar to the working principle of a unified discriminator, DMTG will perform better than the current white-box testing.

Table. 4 illustrates the acceptance levels of different deep learning models towards various curve control parameters. The symbol "×" indicates that the method cannot accept control of the corresponding parameter, while numbers denote the MSE disparity between expected input and generated results. Regarding effective length control, although all models can accept the Mask matrix to constrain the number of effective nodes, SapiAgent exhibits slight jitter at locations where it should remain locked during iterations, leading to its average length exceeding the restriction. This issue also contributes to errors in the starting point control of SapiAgent. In summary, our method can accept all parameter constraints related to curve control, and it outperforms others in maintaining parameter effectiveness.

?? illustrates the disparities between mouse trajectories generated by three deep learning models and Ghost, compared to human data. The blue area represents the distribution of human data, while the red dots depict the distribution of model results. From these results, several observations can be made:

- 1) Compared to SapiAgent and GAN, the data generated by DMTG and Ghost are closer to the distribution of human data.
- 2) **The distribution center of DMTG is closer to the mean of the human distribution.** From the graph, it

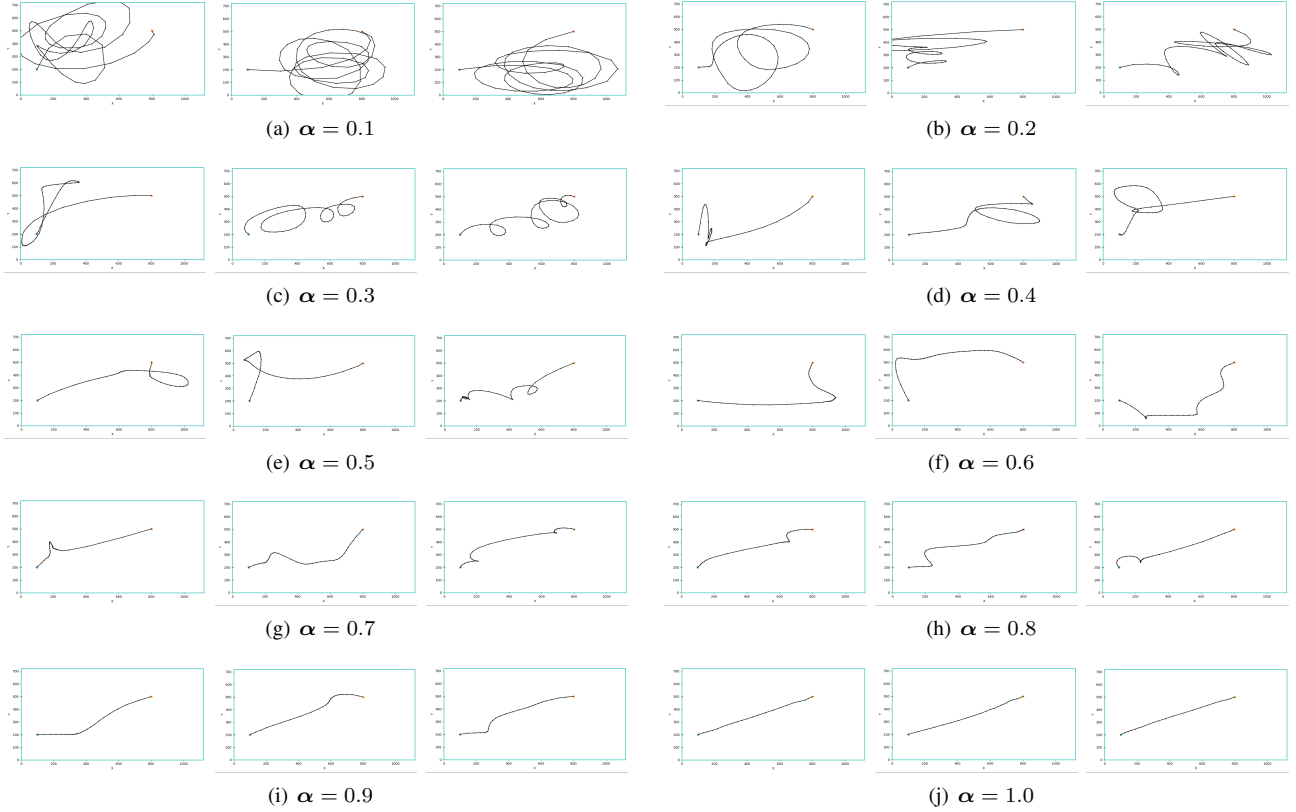


Figure 4. Examples of DMTG Curves under Different α Values in Eq. (10)

TABLE 1. DIFFERENCES IN STATISTICS WITH DIFFERENT α S

Metric	α in Eq. (10)								
	0.0-0.2	0.2-0.4	0.4-0.6	0.6-0.8	0.8-1.0	0.0-0.1	0.1-0.2	0.2-0.3	0.3-0.4
JSD	0.4520	<u>0.4293</u>	0.4560	0.5194	0.5528	0.5659	0.4845	0.3911	0.5131
EMD	6.9235e-4	4.8889e-4	5.1111e-4	6.4444e-4	1.0444e-3	6.1111e-4	9.0000e-4	3.1111e-4	1.2778e-3
MSE	1.1164e+3	9.9901e+2	1.0660e+3	1.0254e+3	1.1488e+3	4.3043e+3	1.7324e+3	1.3168e+3	1.49763+3
RMSE	3.3412e+1	3.1607e+1	3.2650e+1	3.2021e+1	3.3893e+1	6.5638e+1	4.1622e+1	<u>3.6288e+1</u>	3.8699e+1
CosSim	-2.8197e-2	5.0583e-3	-9.8744e-2	-5.4786e-2	-2.0567e-2	<u>-2.4123e-2</u>	-3.4053e-2	-2.4335e-2	-8.8296e-2

is evident that although Ghost and our method both overlap with human data, Ghost’s data is noticeably concentrated at one end of the human distribution area. This results in the overlapping area appearing as one end red and the other end blue. Conversely, the distribution of our model’s results exhibits a higher degree of blending with the human distribution, covering all regions of the human distribution. This is reflected in the graph as DMTG’s distribution “enclosing” the human distribution, displaying an outer layer of red and an inner layer of blue.

Table. 5 displays the discrepancies between the results generated by all models and human data in terms of data statistics. It can be observed that our model consistently ranks favorably across various evaluation metrics, indicating that trajectories generated by DMTG closely resemble those of humans. In addition, DMTG and Ghost exhibit significant

advantages over the other two similarity metrics related to data distribution, such as JSD and EMD. Although there is little difference among the four models in metrics related to node distance and density such as MSE and RMSE, our model still exhibits the smallest errors.

4.2. RQ3: Commercial CAPTCHA Validations

To further verify the effectiveness of DMTG in real-world applications, we tested it on commercial CAPTCHA systems such as GeeTest and Akamai. These evaluations provided valuable insights into the performance of our model. However, due to the copyright and proprietary restrictions involved with these services, we cannot disclose detailed methods and results in this paper. We understand the importance of transparency and plan to provide more detailed analysis in future work when possible.

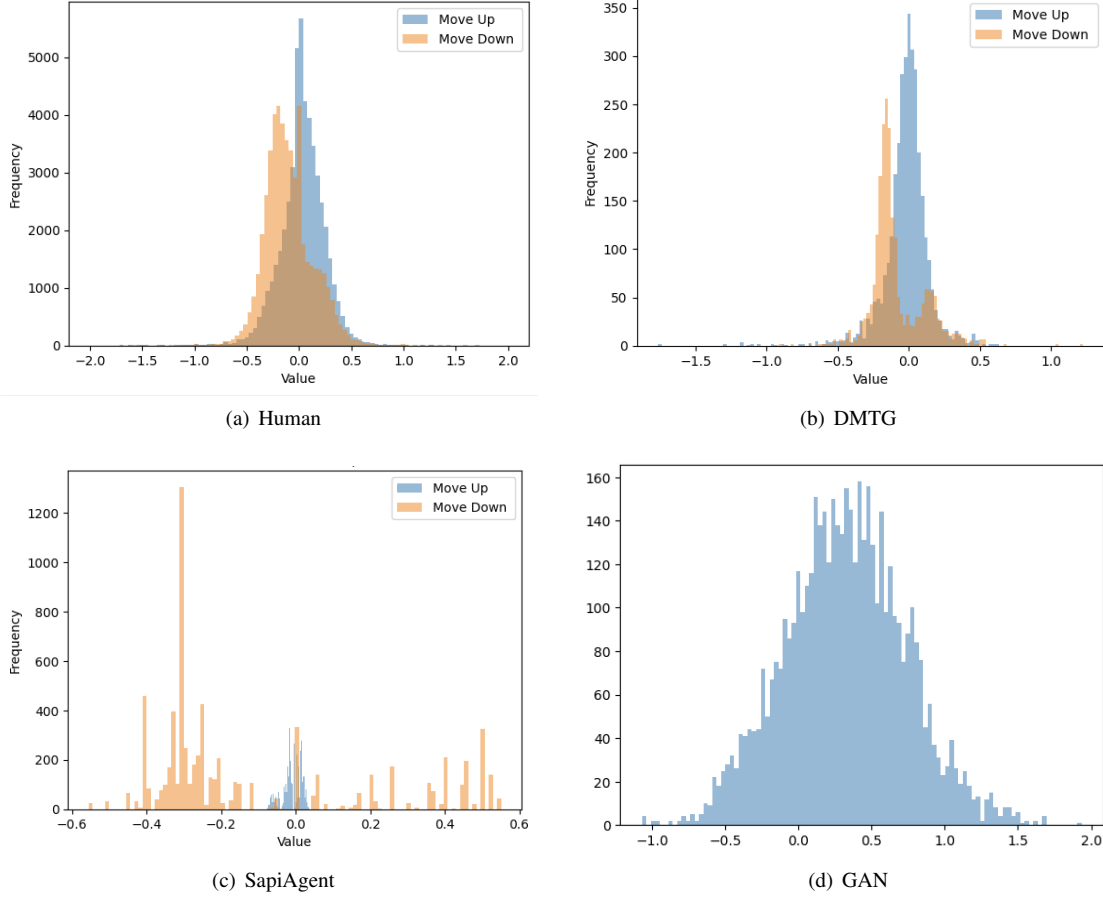


Figure 5. Difference in Acceleration between Upward and Downward Mouse Movements

To understand why our model can generate more realistic trajectories, we conducted a statistical analysis of the acceleration distribution of mouse movements. The comparative results among models are depicted in **Fig. 5**. Except for GAN, all other models can distinguish different movement directions. It is certain that, for humans, the acceleration during upward mouse movements differs from that during downward activation. This discrepancy arises because the force applied to the mouse varies when pushing forward versus pulling backward. Among the models capable of generating random trajectories, only our model can effectively capture this characteristic. This fundamental difference is the reason behind the superior performance of DMTG compared to other models.

4.3. Answers to RQs

For the three research questions we posed, we provide the following answers:

- 1) **Answers to RQ1:** We introduced a mouse trajectory generation method called DMTG, which can control the complexity of curves. It can closely mimic human actions, including acceleration during movement, trajectory uncertainty, and consistency with targets.

- 2) **Answers to RQ2:** We proposed a white-box evaluation method combining mathematical statistics and deep learning to measure the model’s ability to mimic human behavior. This approach accurately captures both global and local features of data distributions, leading to comprehensive evaluation conclusions. Results indicate the superiority of our method across all tests.
- 3) **Answers to RQ3:** We proposed an online CAPTCHA bypass framework and evaluation methods. After the real-world experiments, we found that our method significantly outperforms others in pass rates and nearly achieves human-level performance. This demonstrates the high practical value of our approach.

5. Conclusion

Modern CAPTCHAs have the ability to distinguish between human and bot through mouse trajectory analysis, which does not interrupt user’s experience. In the pursuit of advancing anti-bot research, we have developed a novel contribution to the field of CAPTCHA generation and evaluation. Lacking the capability to exhibit “controllable randomness,” current mouse trajectory generation methods are insufficient in replicating the nuanced variations in human

TABLE 2. PREDICTION INDICATORS OF INDEPENDENT DISCRIMINATORS FOR DISTINGUISHING HUMANS FROM MACHINES

Detector	Generator					
	DMTG	GAN	SapiAgent	Bezier	Ghost	Linear
Accuracy						
DT	0.8759	0.9993	0.9961	0.9776	0.9310	0.9810
RF	0.9149	0.9994	0.9993	0.9845	0.9558	0.9858
GB	0.8912	0.9993	0.9973	0.9624	0.9290	0.9609
XGB	0.9194	0.9996	0.9995	0.9874	0.9608	0.9869
MLP	0.8677	0.9989	0.9932	0.9677	0.9275	0.9861
CNN	0.8920	0.9995	0.9912	0.9869	0.9563	0.9971
RNN	0.8804	0.9976	0.9905	0.9677	0.8900	0.9050
LSTM	0.8709	0.9982	0.9918	0.9729	0.9259	0.9923
BiLSTM	0.9011	0.9940	0.8880	0.9632	0.9646	0.9980
TCN	0.9051	0.9992	0.9957	0.9852	0.9566	0.9881
Macro Precision						
MLP	0.8836	0.9989	0.9932	0.9691	0.9280	0.9865
CNN	0.8944	0.9995	0.9912	0.9870	0.9577	0.9971
RNN	0.8977	0.9976	0.9905	0.9678	0.9095	0.9118
LSTM	0.8846	0.9982	0.9918	0.9738	0.9279	0.9924
BiLSTM	0.9018	0.9940	0.9083	0.9644	0.9648	0.9980
TCN	0.9095	0.9992	0.9957	0.9856	0.9567	0.9883
Macro Recall						
MLP	0.8677	0.9989	0.9932	0.9677	0.9275	0.9861
CNN	0.8920	0.9995	0.9912	0.9869	0.9563	0.9971
RNN	0.8804	0.9976	0.9905	0.9677	0.8900	0.9050
LSTM	0.8709	0.9982	0.9918	0.9729	0.9259	0.9923
BiLSTM	0.9011	0.9940	0.8880	0.9632	0.9646	0.9980
TCN	0.9051	0.9992	0.9957	0.9852	0.9566	0.9881
Macro F1						
MLP	0.8663	0.9989	0.9932	0.9677	0.9274	0.9861
CNN	0.8918	0.9995	0.9912	0.9869	0.9563	0.9971
RNN	0.8791	0.9976	0.9905	0.9677	0.8886	0.9046
LSTM	0.8697	0.9982	0.9918	0.9729	0.9258	0.9923
BiLSTM	0.9010	0.9940	0.8866	0.9632	0.9646	0.9980
TCN	0.9049	0.9992	0.9957	0.9852	0.9566	0.9881

behavior across different testing environments. We propose a mouse trajectory imitation framework based on the entropy-controlled diffusion model: DMTG. This approach has three main tasks: 1) to generate high simulation mouse trajectories like humans; 2) to evaluate the gap between the generated trajectories and humans using white-box testing; and 3) to deploy and participate in online commercial CAPTCHA black-box evaluations. The experimental results demonstrate that our method minimizes the likelihood of detection of robots and closely mimics human operations in terms of data distribution and real-world evaluations. Besides, we have also identified the reasons behind the effectiveness of our method. These reasons include our ability to copy the speed of mouse movements, including slow initiation and differences in acceleration for different directions. Furthermore, our method has the ability to control curve complexity enabling the rapid elimination of significantly discrepant curves during training. The results from our experiments showcase the versatility of our approach and its potential to provide new directions for enhancing anti-bot measures.

TABLE 3. PREDICTION INDICATORS OF UNIFIED DISCRIMINATORS FOR DISTINGUISHING HUMANS FROM MACHINES

Detector	Generator					
	DMTG	GAN	SapiAgent	Bezier	Ghost	Linear
Accuracy						
DT	0.8210	0.9586	0.9548	0.9401	0.8993	0.9416
RF	0.8655	0.9747	0.9736	0.9726	0.9385	0.9724
GB	0.8276	0.9500	0.9331	0.9359	0.8922	0.9333
XGB	0.8763	0.9730	0.9709	0.9745	0.9422	0.9704
MLP	0.7646	0.9481	0.9376	0.9369	0.8370	0.9481
CNN	0.7921	0.9658	0.9599	0.9544	0.9262	0.9567
RNN	0.7257	0.9665	0.8358	0.9323	0.8461	0.9613
LSTM	0.7765	0.9390	0.9376	0.9397	0.9177	0.9554
BiLSTM	0.8145	0.9740	0.9485	0.9594	0.9405	0.9640
TCN	0.8346	0.9636	0.9640	0.9502	0.8900	0.9549
Macro Precision						
MLP	0.7852	0.9523	0.9399	0.9390	0.8417	0.9521
CNN	0.8169	0.9677	0.9623	0.9575	0.9255	0.9600
RNN	0.7991	0.9683	0.8475	0.9355	0.8707	0.9617
LSTM	0.8012	0.9447	0.9431	0.9403	0.9177	0.9577
BiLSTM	0.8317	0.9752	0.9494	0.9608	0.9407	0.9661
TCN	0.8453	0.9659	0.9659	0.9529	0.8906	0.9582
Macro Recall						
MLP	0.7646	0.9481	0.9376	0.9369	0.8370	0.9481
CNN	0.7921	0.9658	0.9599	0.9544	0.9262	0.9567
RNN	0.7257	0.9665	0.8358	0.9323	0.8461	0.9613
LSTM	0.7765	0.9390	0.9376	0.9397	0.9177	0.9554
BiLSTM	0.8145	0.9740	0.9485	0.9594	0.9405	0.9640
TCN	0.8346	0.9636	0.9640	0.9502	0.8900	0.9549
Macro F1						
MLP	0.7603	0.9480	0.9376	0.9369	0.8365	0.9480
CNN	0.7879	0.9658	0.9598	0.9543	0.9252	0.9566
RNN	0.7078	0.9665	0.8344	0.9321	0.8435	0.9613
LSTM	0.7718	0.9388	0.9364	0.9397	0.9177	0.9553
BiLSTM	0.8121	0.9740	0.9485	0.9593	0.9405	0.9640
TCN	0.8333	0.9636	0.9639	0.9502	0.8900	0.9548

TABLE 4. ADAPTATION AND RETENTION OF PARAMETER CONTROLS FOR EACH GENERATING MODEL BASED ON DEEP LEARNINGS

Model	Control Parameter		
	Effective Length	Start & End Points	Complexity
DMTG	0	8.2784e-10	0.0179
SapiAgent	102	0.3383	×
GAN	0	×	×

TABLE 5. DIFFERENCES IN STATISTICS BETWEEN MOUSE TRAJECTORIES OF HUMANS AND VARIOUS MODELS ON DATA DISTRIBUTION

Metric	Generator			
	DMTG	GAN	Ghost	SapiAgent
JSD	0.3025	0.5865	0.3565	0.6325
EMD	1.5170e-4	7.9644e-4	2.5896e-4	1.4080e-3
MSE	5.5919e+3	6.5803e+3	6.0058e+3	6.6803e+3
RMSE	7.4779e+1	8.1191e+1	7.7497e+1	8.1733e+1
CosSim	-0.0130	-0.1829	-0.0130	-0.1356

References

- [1] X. Xu, L. Liu, and B. Li, "A survey of captcha technologies to distinguish between human and computer," *Neurocomputing*, vol. 408, pp. 292–307, 2020. [Online]. Available: <https://www.sciencedirect.com/science/article/pii/S0925231220304896>
- [2] Y. Gao, H. Gao, S. Luo, Y. Zi, S. Zhang, W. Mao, P. Wang, Y. Shen, and J. Yan, "Research on the security of visual reasoning CAPTCHA," in *30th USENIX Security Symposium (USENIX Security 21)*. USENIX Association, Aug. 2021, pp. 3291–3308. [Online]. Available: <https://www.usenix.org/conference/usenixsecurity21/presentation/gao>
- [3] P. Wang, H. Gao, C. Xiao, X. Guo, Y. Gao, and Y. Zi, "Extended research on the security of visual reasoning captcha," *IEEE Transactions on Dependable and Secure Computing*, vol. 20, no. 6, pp. 4976–4992, 2023.
- [4] C. Li, X. Chen, H. Wang, P. Wang, Y. Zhang, and W. Wang, "End-to-end attack on text-based captchas based on cycle-consistent generative adversarial network," *Neurocomputing*, vol. 433, pp. 223–236, 2021. [Online]. Available: <https://www.sciencedirect.com/science/article/pii/S0925231220318518>
- [5] P. Wang, H. Gao, X. Guo, C. Xiao, F. Qi, and Z. Yan, "An experimental investigation of text-based captcha attacks and their robustness," *ACM Comput. Surv.*, vol. 55, no. 9, jan 2023. [Online]. Available: <https://doi.org/10.1145/3559754>
- [6] R. Zhao, X. Deng, Y. Wang, Z. Yan, Z. Han, L. Chen, Z. Xue, and Y. Wang, "Geesolver: A generic, efficient, and effortless solver with self-supervised learning for breaking text captchas," in *2023 IEEE Symposium on Security and Privacy (SP)*, 2023, pp. 1649–1666.
- [7] T. Diwan, G. Anirudh, and J. V. Tembhurne, "Object detection using yolo: Challenges, architectural successors, datasets and applications," *multimedia Tools and Applications*, vol. 82, no. 6, pp. 9243–9275, 2023.
- [8] G. Deng, H. Ou, Y. Liu, J. Zhang, T. Zhang, and Y. Liu, "Oedipus: Llm-enhanced reasoning captcha solver," *arXiv preprint arXiv:2405.07496*, 2024.
- [9] A. Acien, A. Morales, J. Fierrez, and R. Vera-Rodriguez, "Becaptcha-mouse: Synthetic mouse trajectories and improved bot detection," *Pattern Recognition*, vol. 127, p. 108643, 2022. [Online]. Available: <https://www.sciencedirect.com/science/article/pii/S0031320322001248>
- [10] I. Akrou, A. Feriani, and M. Akrou, "Hacking google recaptcha v3 using reinforcement learning," *arXiv preprint arXiv:1903.01003*, 2019.
- [11] I. Tsingenopoulos, D. Preuveneers, L. Desmet, and W. Joosen, "Captcha me if you can: Imitation games with reinforcement learning," in *2022 IEEE 7th European Symposium on Security and Privacy (EuroS&P)*, 2022, pp. 719–735.
- [12] P. C. Humphreys, D. Raposo, T. Pohlen, G. Thornton, R. Chhaparia, A. Muldal, J. Abramson, P. Georgiev, A. Santoro, and T. Lillicrap, "A data-driven approach for learning to control computers," in *Proceedings of the 39th International Conference on Machine Learning*, ser. *Proceedings of Machine Learning Research*, K. Chaudhuri, S. Jegelka, L. Song, C. Szepesvari, G. Niu, and S. Sabato, Eds., vol. 162. PMLR, 17–23 Jul 2022, pp. 9466–9482. [Online]. Available: <https://proceedings.mlr.press/v162/humphreys22a.html>
- [13] M. Antal, K. Buza, and N. Fejer, "Sapiagent: A bot based on deep learning to generate human-like mouse trajectories," *IEEE Access*, vol. 9, pp. 124 396–124 408, 2021.
- [14] S. Zhao, J. Fang, S. Zhao, R. Wu, J. Tao, S. Li, and G. Pan, "T-detector: A trajectory based pre-trained model for game bot detection in mmorpgs," in *2022 IEEE 38th International Conference on Data Engineering (ICDE)*, 2022, pp. 992–1003.
- [15] J. Song, C. Meng, and S. Ermon, "Denoising diffusion implicit models," in *International Conference on Learning Representations*, 2021. [Online]. Available: <https://openreview.net/forum?id=St1giarCHLP>
- [16] H. Wang, F. Zheng, Z. Chen, Y. Lu, J. Gao, and R. Wei, "A captcha design based on visual reasoning," in *2018 IEEE International Conference on Acoustics, Speech and Signal Processing (ICASSP)*, 2018, pp. 1967–1971.
- [17] Google, "What is recaptcha?" 2 2024. [Online]. Available: <https://developers.google.com/recaptcha>
- [18] S. Yilmaz, S. Zavrak, and H. Bodur, "Distinguishing humans from automated programs by a novel audio-based captcha," *International Journal of Computer Applications*, vol. 132, pp. 17–21, 12 2015.
- [19] R. Jin, L. Huang, J. Duan, W. Zhao, Y. Liao, and P. Zhou, "How secure is your website? a comprehensive investigation on captcha providers and solving services," *arXiv preprint arXiv:2306.07543*, 2023.
- [20] M. I. Hossen, Y. Tu, M. F. Rabby, M. N. Islam, H. Cao, and X. Hei, "An object detection based solver for Google's image reCAPTCHA v2," in *23rd International Symposium on Research in Attacks, Intrusions and Defenses (RAID 2020)*. San Sebastian: USENIX Association, Oct. 2020, pp. 269–284. [Online]. Available: <https://www.usenix.org/conference/raid2020/presentation/hossen>
- [21] J. Redmon and A. Farhadi, "Yolov3: An incremental improvement," *arXiv preprint arXiv:1804.02767*, 2018.
- [22] P. Wang, H. Gao, Q. Rao, S. Luo, Z. Yuan, and Z. Shi, "A security analysis of captchas with large character sets," *IEEE Transactions on Dependable and Secure Computing*, vol. 18, no. 6, pp. 2953–2968, 2021.
- [23] M. Schuster and K. Paliwal, "Bidirectional recurrent neural networks," *IEEE Transactions on Signal Processing*, vol. 45, no. 11, pp. 2673–2681, 1997.
- [24] Z. Li, F. Liu, W. Yang, S. Peng, and J. Zhou, "A survey of convolutional neural networks: Analysis, applications, and prospects," *IEEE Transactions on Neural Networks and Learning Systems*, vol. 33, no. 12, pp. 6999–7019, 2022.
- [25] A. Vaswani, N. Shazeer, N. Parmar, J. Uszkoreit, L. Jones, A. N. Gomez, L. u. Kaiser, and I. Polosukhin, "Attention is all you need," in *Advances in Neural Information Processing Systems*, I. Guyon, U. V. Luxburg, S. Bengio, H. Wallach, R. Fergus, S. Vishwanathan, and R. Garnett, Eds., vol. 30. Curran Associates, Inc., 2017.
- [26] G. Zhang, Z. Hu, M. Bâce, and A. Bulling, "Mouse2vec: Learning reusable semantic representations of mouse behaviour," in *Proceedings of the CHI Conference on Human Factors in Computing Systems*, ser. *CHI '24*. New York, NY, USA: Association for Computing Machinery, 2024. [Online]. Available: <https://doi.org/10.1145/3613904.3642141>
- [27] S. Sadeghpour and N. Vlajic, "Remouse dataset: On the efficacy of measuring the similarity of human-generated trajectories for the detection of session-replay bots," *Journal of Cybersecurity and Privacy*, vol. 3, no. 1, pp. 95–117, 2023. [Online]. Available: <https://www.mdpi.com/2624-800X/3/1/7>
- [28] A. Acien, A. Morales, R. Vera-Rodriguez, and J. Fierrez, "Smart-phone sensors for modeling human-computer interaction: General outlook and research datasets for user authentication," in *2020 IEEE 44th Annual Computers, Software, and Applications Conference (COMPSAC)*, 2020, pp. 1273–1278.
- [29] R. Jin, Y. Liao, and P. Zhou, "User authentication and identity inconsistency detection via mouse-trajectory similarity measurement," *arXiv preprint arXiv:2312.10273*, 2023.
- [30] I. Goodfellow, J. Pouget-Abadie, M. Mirza, B. Xu, D. Warde-Farley, S. Ozair, A. Courville, and Y. Bengio, "Generative adversarial nets," in *Advances in Neural Information Processing Systems*, Z. Ghahramani, M. Welling, C. Cortes, N. Lawrence, and K. Weinberger, Eds., vol. 27. Curran Associates, Inc., 2014.

- [31] S. E. Folch, A. C. Ibáñez, N. O. Rabella, and J. E. Escrig, "Web bot detection using mouse movement," in *2023 JNIC Cybersecurity Conference (JNIC)*, 2023, pp. 1–6.
- [32] E. Z. Liu, K. Guu, P. Pasupat, T. Shi, and P. Liang, "Reinforcement learning on web interfaces using workflow-guided exploration," *arXiv preprint arXiv:1802.08802*, 2018.
- [33] L. P. Kaelbling, M. L. Littman, and A. W. Moore, "Reinforcement learning: A survey," *Journal of artificial intelligence research*, vol. 4, pp. 237–285, 1996.
- [34] S. Noy and W. Zhang, "Experimental evidence on the productivity effects of generative artificial intelligence," *Science*, vol. 381, no. 6654, pp. 187–192, 2023. [Online]. Available: <https://www.science.org/doi/abs/10.1126/science.adh2586>
- [35] D. Baidoo-anu and L. Owusu Ansah, "Education in the era of generative artificial intelligence (ai): Understanding the potential benefits of chatgpt in promoting teaching and learning," *Journal of AI*, vol. 7, no. 1, p. 52–62, 2023.
- [36] C.-Y. Liou, W.-C. Cheng, J.-W. Liou, and D.-R. Liou, "Autoencoder for words," *Neurocomputing*, vol. 139, pp. 84–96, 2014. [Online]. Available: <https://www.sciencedirect.com/science/article/pii/S0925231214003658>
- [37] D. P. Kingma and M. Welling, "Auto-encoding variational bayes," *arXiv preprint arXiv:1312.6114*, 2013.
- [38] P. Vincent, H. Larochelle, Y. Bengio, and P.-A. Manzagol, "Extracting and composing robust features with denoising autoencoders," in *Proceedings of the 25th International Conference on Machine Learning*, ser. ICML '08. New York, NY, USA: Association for Computing Machinery, 2008, p. 1096–1103. [Online]. Available: <https://doi.org/10.1145/1390156.1390294>
- [39] Z. Qin, W. Zhao, X. Yu, and X. Sun, "Openvoice: Versatile instant voice cloning," *arXiv preprint arXiv:2312.01479*, 2023.
- [40] I. Goodfellow, J. Pouget-Abadie, M. Mirza, B. Xu, D. Warde-Farley, S. Ozair, A. Courville, and Y. Bengio, "Generative adversarial networks," *Commun. ACM*, vol. 63, no. 11, p. 139–144, oct 2020. [Online]. Available: <https://doi.org/10.1145/3422622>
- [41] J.-Y. Zhu, T. Park, P. Isola, and A. A. Efros, "Unpaired image-to-image translation using cycle-consistent adversarial networks," in *Proceedings of the IEEE International Conference on Computer Vision (ICCV)*, 2017, pp. 2223–2232.
- [42] T. Karras, S. Laine, and T. Aila, "A style-based generator architecture for generative adversarial networks," in *Proceedings of the IEEE/CVF conference on computer vision and pattern recognition*, 2019, pp. 4401–4410.
- [43] K. Han, Y. Wang, H. Chen, X. Chen, J. Guo, Z. Liu, Y. Tang, A. Xiao, C. Xu, Y. Xu, Z. Yang, Y. Zhang, and D. Tao, "A survey on vision transformer," *IEEE Transactions on Pattern Analysis and Machine Intelligence*, vol. 45, no. 1, pp. 87–110, 2023.
- [44] T. Brown, B. Mann, N. Ryder, M. Subbiah, J. D. Kaplan, P. Dhariwal, A. Neelakantan, P. Shyam, G. Sastry, A. Askell et al., "Language models are few-shot learners," *Advances in neural information processing systems*, vol. 33, pp. 1877–1901, 2020.
- [45] A. Ramesh, M. Pavlov, G. Goh, S. Gray, C. Voss, A. Radford, M. Chen, and I. Sutskever, "Zero-shot text-to-image generation," in *Proceedings of the 38th International Conference on Machine Learning*, ser. Proceedings of Machine Learning Research, M. Meila and T. Zhang, Eds., vol. 139. PMLR, 18–24 Jul 2021, pp. 8821–8831. [Online]. Available: <https://proceedings.mlr.press/v139/ramesh21a.html>
- [46] J. Sohl-Dickstein, E. Weiss, N. Maheswaranathan, and S. Ganguli, "Deep unsupervised learning using nonequilibrium thermodynamics," in *Proceedings of the 32nd International Conference on Machine Learning*, ser. Proceedings of Machine Learning Research, F. Bach and D. Blei, Eds., vol. 37. Lille, France: PMLR, 07–09 Jul 2015, pp. 2256–2265. [Online]. Available: <https://proceedings.mlr.press/v37/sohl-dickstein15.html>
- [47] J. Ho, A. Jain, and P. Abbeel, "Denoising diffusion probabilistic models," in *Advances in Neural Information Processing Systems*, H. Larochelle, M. Ranzato, R. Hadsell, M. Balcan, and H. Lin, Eds., vol. 33. Curran Associates, Inc., 2020, pp. 6840–6851.
- [48] J. Abramson, J. Adler, J. Dunger, R. Evans, T. Green, A. Pritzel, O. Ronneberger, L. Willmore, A. J. Ballard, J. Bambrick et al., "Accurate structure prediction of biomolecular interactions with alphafold 3," *Nature*, pp. 1–3, 5 2024. [Online]. Available: <https://doi.org/10.1038/s41586-024-07487-w>
- [49] H. Touvron, T. Lavril, G. Izacard, X. Martinet, M.-A. Lachaux, T. Lacroix, B. Rozière, N. Goyal, E. Hambro, F. Azhar et al., "Llama: Open and efficient foundation language models," *arXiv preprint arXiv:2302.13971*, 2023.
- [50] S. R. Dubey and S. K. Singh, "Transformer-based generative adversarial networks in computer vision: A comprehensive survey," *IEEE Transactions on Artificial Intelligence*, pp. 1–16, 2024.
- [51] L. Papa, P. Russo, I. Amerini, and L. Zhou, "A survey on efficient vision transformers: Algorithms, techniques, and performance benchmarking," *IEEE Transactions on Pattern Analysis and Machine Intelligence*, pp. 1–20, 2024.
- [52] J. Wu, W. Ji, H. Fu, M. Xu, Y. Jin, and Y. Xu, "Medsegdiff-v2: Diffusion-based medical image segmentation with transformer," in *Proceedings of the AAAI Conference on Artificial Intelligence*, vol. 38, no. 6, 3 2024, pp. 6030–6038. [Online]. Available: <https://ojs.aaai.org/index.php/AAAI/article/view/28418>
- [53] O. Ronneberger, P. Fischer, and T. Brox, "U-net: Convolutional networks for biomedical image segmentation," *arXiv preprint arXiv:1505.04597*, 2015.
- [54] F. Bao, S. Nie, K. Xue, C. Li, S. Pu, Y. Wang, G. Yue, Y. Cao, H. Su, and J. Zhu, "One transformer fits all distributions in multi-modal diffusion at scale," in *Proceedings of the 40th International Conference on Machine Learning*, ser. Proceedings of Machine Learning Research, A. Krause, E. Brunskill, K. Cho, B. Engelhardt, S. Sabato, and J. Scarlett, Eds., vol. 202. PMLR, 23–29 Jul 2023, pp. 1692–1717. [Online]. Available: <https://proceedings.mlr.press/v202/bao23a.html>
- [55] H. Cao, C. Tan, Z. Gao, Y. Xu, G. Chen, P.-A. Heng, and S. Z. Li, "A survey on generative diffusion models," *IEEE Transactions on Knowledge and Data Engineering*, pp. 1–20, 2024.
- [56] F.-A. Croitoru, V. Hondru, R. T. Ionescu, and M. Shah, "Diffusion models in vision: A survey," *IEEE Transactions on Pattern Analysis and Machine Intelligence*, vol. 45, no. 9, pp. 10 850–10 869, 2023.
- [57] L. Yang, Z. Zhang, Y. Song, S. Hong, R. Xu, Y. Zhao, W. Zhang, B. Cui, and M.-H. Yang, "Diffusion models: A comprehensive survey of methods and applications," *ACM Comput. Surv.*, vol. 56, no. 4, nov 2023. [Online]. Available: <https://doi.org/10.1145/3626235>
- [58] M. Antal, N. Fejér, and K. Buza, "Sapimouse: Mouse dynamics-based user authentication using deep feature learning," in *2021 IEEE 15th International Symposium on Applied Computational Intelligence and Informatics (SACI)*, 2021, pp. 61–66.
- [59] A. Kuznetsova, H. Rom, N. Alldrin, J. Uijlings, I. Krasin, J. Pont-Tuset, S. Kamali, S. Popov, M. Mallocci, A. Kolesnikov et al., "The open images dataset v4: Unified image classification, object detection, and visual relationship detection at scale," *International journal of computer vision*, vol. 128, no. 7, pp. 1956–1981, 2020.
- [60] M. Menéndez, J. Pardo, L. Pardo, and M. Pardo, "The jensen-shannon divergence," *Journal of the Franklin Institute*, vol. 334, no. 2, pp. 307–318, 1997. [Online]. Available: <https://www.sciencedirect.com/science/article/pii/S0016003296000634>
- [61] V. M. Panaretos and Y. Zemel, "Statistical aspects of wasserstein distances," *Annual Review of Statistics and Its Application*, vol. 6, pp. 405–431, 2019. [Online]. Available: <https://www.annualreviews.org/content/journals/10.1146/annurev-statistics-030718-104938>
- [62] Y. Rubner, C. Tomasi, and L. J. Guibas, "The earth mover's distance as a metric for image retrieval," *International journal of computer vision*, vol. 40, pp. 99–121, 2000.

- [63] L. van der Maaten and G. Hinton, “Visualizing data using t-sne,” *Journal of Machine Learning Research*, vol. 9, no. 86, pp. 2579–2605, 2008. [Online]. Available: <http://jmlr.org/papers/v9/vandemaaten08a.html>
- [64] Akamai, “Power and protect life online,” 2024. [Online]. Available: <https://www.akamai.com/why-akamai>
- [65] GeeTest, “Geetest captcha v3,” 2024. [Online]. Available: <https://www.geetest.com/en/Captcha>
- [66] H. Prautzsch, W. Boehm, and M. Paluszny, *Bézier and B-spline techniques*. Springer, 2002, vol. 6. [Online]. Available: <https://doi.org/10.1007/978-3-662-04919-8>
- [67] Xetera, “Ghost cursor,” 2024. [Online]. Available: <https://github.com/Xetera/ghost-cursor>
- [68] Y.-Y. Song and L. Ying, “Decision tree methods: applications for classification and prediction,” *Shanghai archives of psychiatry*, vol. 27, no. 2, p. 130–135, 2015.
- [69] L. Breiman, “Random forests,” *Machine learning*, vol. 45, pp. 5–32, 2001.
- [70] A. Ogunleye and Q.-G. Wang, “Xgboost model for chronic kidney disease diagnosis,” *IEEE/ACM Transactions on Computational Biology and Bioinformatics*, vol. 17, no. 6, pp. 2131–2140, 2020.
- [71] C. Bentéjac, A. Csörgő, and G. Martínez-Muñoz, “A comparative analysis of gradient boosting algorithms,” *Artificial Intelligence Review*, vol. 54, pp. 1937–1967, 2021.
- [72] A. Pinkus, “Approximation theory of the mlp model in neural networks,” *Acta Numerica*, vol. 8, p. 143–195, 1999.
- [73] A. Graves, *Long Short-Term Memory*. Berlin, Heidelberg: Springer Berlin Heidelberg, 2012, pp. 37–45. [Online]. Available: https://doi.org/10.1007/978-3-642-24797-2_4
- [74] S. Zhang, D. Zheng, X. Hu, and M. Yang, “Bidirectional long short-term memory networks for relation classification,” in *Proceedings of the 29th Pacific Asia conference on language, information and computation*, 2015, pp. 73–78.
- [75] S. Bai, J. Z. Kolter, and V. Koltun, “An empirical evaluation of generic convolutional and recurrent networks for sequence modeling,” *arXiv preprint arXiv:1803.01271*, 2018.

Appendix

Fig. 6 presents the disparities between the four models in data distribution compared to human behavior, serving as supplementary material to ???. On the left side are the t-SNE-compressed data distributions of the models, while on the right side are the corresponding human distributions. It can be observed that SapiAgent and GAN models hardly overlap with the human distribution. DMTG’s distribution exhibits fewer voids compared to Ghost, indicating more uniform sampling in this mapping.

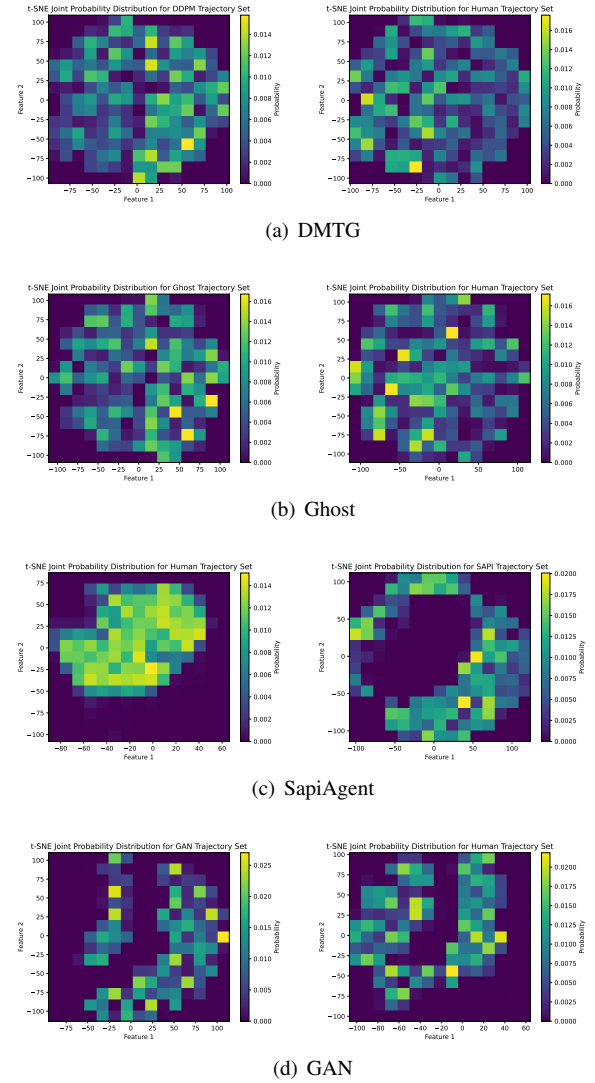


Figure 6. Similarities between Sampling Probability of Human Mouse Trajectories and Models’